

---

# MARKOV-LIPSCHITZ DEEP LEARNING

---

Stan Z. Li    Zelin Zhang    Lirong Wu

School of Engineering, Westlake University &  
Institute of Advanced Technology, Westlake Institute for Advanced Study  
Hangzhou, Zhejiang, China

June 21, 2022

## ABSTRACT

In this paper, we propose a novel framework, called Markov-Lipschitz deep learning (MLDL), for manifold learning and data generation. It enhances layer-wise transformations of neural networks by optimizing isometry (geometry-preserving) and stability of the mappings. A prior constraint of *locally isometric smoothness* (LIS) is imposed across-layers and encoded via a Markov random field (MRF)-Gibbs distribution, and consequently layer-wise vector transformations are replaced by LIS-constrained metric homeomorphisms. These lead to the best possible solutions as measured by locally geometric distortion and locally bi-Lipschitz continuity. Extensive experiments, comparisons and ablation study demonstrate significant advantages of MLDL for manifold learning and data generation.

## 1 Introduction

The manifold assumption hypothesizes that data of a meaningful pattern lives in a low dimensional manifold embedded in a higher dimensional space (Belkin & Niyogi, 2003; Fefferman et al., 2016). We wish to develop a nonlinear dimensionality reduction (NLDR) mapping to transform the data from the input data space to a latent space where we can the Euclidean metric to facilitate pattern analysis. There are numerous literature on manifold learning for NLDR, including classic algorithms ISOMAP [28] using multidimensional scaling (MDS), LLE [27], which are further developed with local MDS in [7, 10, 22]. Preserving local geometric structure is a key to its success.

Geometric deep learning (GDL) [5] attempts to generalize (structured) deep neural models to non-Euclidean domains such as graphs and manifolds. Topological data analysis (TDA) [30] integrates applied topology and computational geometry in a way that is insensitive to the particular metric chosen, such as using persistent homology [16, 6, 23]. GDL is more interested in manifold and embedding learning based on local geometry whereas TDA is more about the global topology.

The Lipschitz continuity theory is a tool for analyzing the stability of mappings from one metric space to another in which the Lipschitz constant may be used as a measure of instability. Recent years have seen interest in using Lipschitz continuity to improve neural networks in generalization [3, 1], robustness against adversarial attacks [31, 8], and generative modeling [?, 25]. Supporting this research are efficient algorithms for estimation of the Lipschitz constant [29, ?, 19]. For local neighborhood-based manifold learning, we believe local Lipschitz continuity is more interesting.

The Markov random field (MRF) theory is a tool for modeling data with respect to a local neighborhood system [13, 4]. Incorporation of MRF priors into the *maximum a posteriori* (MAP) estimation gives rise to the principled MAP-MRF approach [11, 20] for developing a variety of statistical models. Among these are surface reconstruction, image denoising and inexact Bayesian shape matching [20]. In recent year, MRFs have been incorporated into deep neural networks [26, 17, 2, 32, 12].

In this paper, we develop a novel deep learning framework, called Markov-Lipschitz deep learning (MLDL), for manifold learning, NLDR, and data generation. The motivations are the following: First, we believe that layer-wise vector transformations should be enhanced by *metric homeomorphisms* to make the neural mappings better behaved. Second, while manifold learning relies on local geometry structures of data samples with respect to neighborhood

systems at various levels, such structures may be modeled by *Markov random fields or MRFs* locally and equivalently by MRF-Gibbs distributions globally. Third, it is desirable to impose a local geometry preserving or isometric constraint on layer-wise neural homeomorphisms for purposes of both manifold learning and network stability and robustness and this may be done by using *locally bi-Lipschitz continuity* encoded in the MRF-Gibbs distribution as energy or loss functions. The main contributions, to the best of our knowledge, are summarized below:

- (1) Proposing the MLDL framework that imposes the prior constraint of *locally isometric smoothness* (LIS) on cross-layer homeomorphic transformations and encodes the LIS into an MRF-Gibbs prior distribution. This results in MLDL neural networks optimized in terms of not only local geometry preservation as measured by the geometric distortion, but also homeomorphic regularity as measured by the locally bi-Lipschitz constant.
- (2) Proposing two instances of MLDL-based neural networks: the Markov-Lipschitz Encoder (**ML-Enc**) for manifold learning, and the Markov-Lipschitz AutoEncoder (**ML-AE**) for manifold data generation.
- (3) Proposing an auxiliary term for manifold learning. It effectively helps prevent MLDL training from falling into a bad local optimum.
- (4) Providing extensive experiments, with self- and comparative evaluations and ablation study. The results clearly demonstrate significant advantages of MLDL over existing methods.

The rest of the paper is organized as follows: Section 2 introduces the MLDL network structure and related preliminaries. Section 3 presents the two MLDL neural networks (ML-Enc and ML-AE). Section 4 presents extensive experiments. Section 5 makes conclusions. More details of experiments can be found in Appendix.

## 2 MLDL structure and homeomorphisms

The structure of MLDL networks is outlined in Fig. 1. There, the ML-Encoder, composed of a cascade of  $L$  locally homeomorphic transformations, is aimed for manifold and embedding learning, and the corresponding  $L$ -layer ML-Decoder for reconstruction and data generation. MLDL also supports supervised and semi-supervised tasks such as classification (not developed in this paper). In this work, the locality is modeled by MRFs and the imposition of the cross-layer LIS constraint leads to desired locally Lipschitz properties. This section introduces MRF preliminaries and describes local homeomorphisms for MLDL.

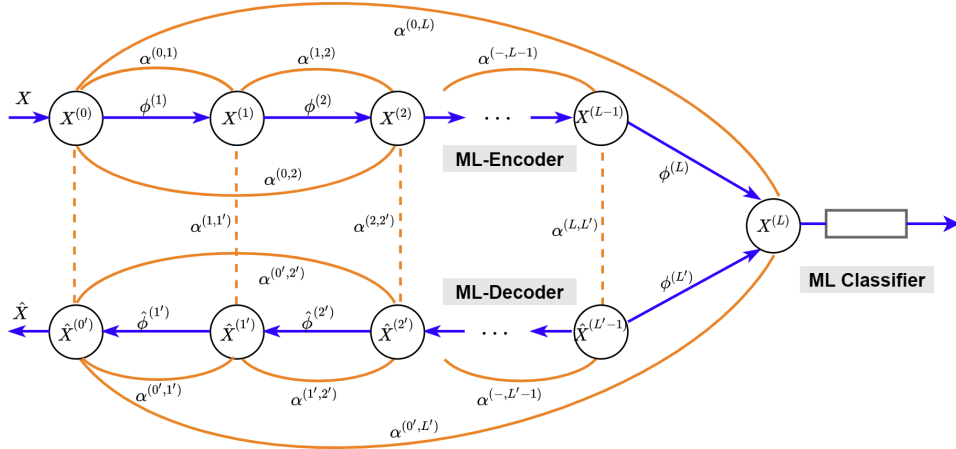


Figure 1: MLDL neural networks consists of a cascade of layer-wise homeomorphisms connected by arrows in blue. The LIS prior constraint on the homeomorphisms are imposed across-layers, shown as arcs and dashed lines in orange. The LIS constraint are encoded into an MRF-Gibbs distribution in the form of energy (loss) functions.

### 2.1 MRFs on neural networks

**MRF on data samples.** Let  $X = \{x_1, \dots, x_M\}$  be a set of samples on a manifold  $\mathcal{M}_X$  embedded in  $\mathbb{R}^N$ , with  $X \subset \mathcal{M}_X \subset \mathbb{R}^N$ , and  $d_X$  be a metric on  $X$  so that  $(X, d_X)$  is a metric space. Let  $\mathcal{S} := \{1, \dots, M\}$  be the set of indices. The neighborhood of  $x_i$  can be defined by its  $k$ -nearest neighbors or the  $r$ -ball centered at  $x_i$ . Let  $\mathcal{N}_i = \{j \in \mathcal{S} | x_j \in B_r(x_i)\}$  be the index of the neighbors of  $x_i$  and  $\mathcal{N} = \{\mathcal{N}_i | \forall i \in \mathcal{S}\}$  be the neighborhood system.

The tangent subspace  $T_x(\mathcal{M}_X)$  of the manifold at any  $x \in \mathcal{M}_X$  is locally isomorphic to the Euclidean space of  $\dim(\mathcal{M}_X)$ . While the above specifications are for the input (layer), they apply to another space after a  $C^0$ -continuous transformation. In this paper, we use the Euclidean metric for every space; when we write a pair  $(i, j) \in \mathcal{S} \times \mathcal{S}$ , it is limited by  $j \in \mathcal{N}_i$ , unless specified otherwise.

$X$  is said to be an MRF on  $\mathcal{S}$  with respect to  $\mathcal{N}$  if the Markovian condition  $p(x_i | X_{\mathcal{S}-\{i\}}) = p(x_i | X_{\mathcal{N}_i})$ , where  $X_{\mathcal{S}-\{i\}} = \{x_j | j \in \mathcal{S} - \{i\}\}$  and  $X_{\mathcal{N}_i} = \{x_j | j \in \mathcal{N}_i\}$ , and the positivity condition  $p(X) > 0$  ( $\forall X$ ) are satisfied. The joint distribution of an MRF can be formulated according to a theorem of MRF-Gibbs equivalence [13, 4, 11]. The theorem states that  $X$  is an MRF on  $\mathcal{S}$  with respect to  $\mathcal{N}$  if and only if its joint distribution  $P(X)$  is a Gibbs distribution with respect to  $\mathcal{N}$ .

A Gibbs distribution (GD) of  $X$  is featured by two things: (1) it belongs to the exponential family; (2) its energy function is defined on given cliques. A clique consists of either a single node  $\{i\}$  or a pair of neighboring nodes  $\{i, j\}$ . Let's denote the respective set by  $\mathcal{C}_1 = \{\{i\} | i \in \mathcal{S}\}$  and  $\mathcal{C}_2 = \{\{i, j\} | j \in \mathcal{N}_i, i \in \mathcal{S}\}$  and the collection of all given cliques by  $\mathcal{C} = \mathcal{C}_1 \cup \mathcal{C}_2$ . A GD of  $X$  with respect to  $\mathcal{N}$  is of the following form

$$p(X) = \Xi^{-1} \times e^{-U(X)/T},$$

where  $U(X) = \sum_{c \in \mathcal{C}} V_c(X)$  is the energy composed of clique potentials  $V_c(X)$ ,  $T$  is a global parameter called the temperature and  $\Xi$  the normalizing constant.

**MRF on network layers.** Consider an  $L$ -layer neural network such as the ML encoder in Fig. 1. Let  $\tilde{X} = \{X^{(0)}, X^{(1)}, \dots, X^{(L)}\}$ , with  $X^{(0)} = X$  (the input), and  $\mathcal{S}_L = \{0, \dots, L\}$ .  $\tilde{X}$  is an MRF on  $\mathcal{S}_L$  if the above two conditions are satisfied. Let  $\Lambda_L = \{(l, l') | l < l', l \in \mathcal{S}_L\}$  be the set of all cross-layer (undirected) links, which we call super-cliques, and  $\Lambda \subseteq \Lambda_L$  be a subset under consideration. Underlying  $\Lambda$  is a neighborhood system  $\mathcal{N}_L$  independent of the input data. In the MLDL framework, the prior LIS constraint is encoded into cross-layer super-clique potentials which are then summed over all  $\lambda = (l, l') \in \Lambda$  into the energy function of a for the MRF-Gibbs prior distribution

$$U(\tilde{X}) = \sum_{\lambda \in \Lambda} V_\lambda(\tilde{X}).$$

Although not developed in this paper, imposition of prior knowledge via a MRF-Gibbs prior distribution can provide a tool for formulating a deep learning problem in a principled way such as *maximum a posteriori* (MAP) estimation.

## 2.2 Local homeomorphisms

**Transformation between graphs.** Manifold learning is associated with local geometric structure of data defined by a neighborhood system. It can be done by analyzing the graph  $\mathcal{G}(X, D, \mathcal{N})$ , in which  $D = [d(x_i, x_j)]$  is the distance matrix providing quantitative information about local neighborhood. The data generation process is assumed to be a local homeomorphism (a mapping from one manifold to another)

$$\Psi : \mathcal{G}(Z, D^Z, \mathcal{N}^Z) \rightarrow \mathcal{G}(X, D^X, \mathcal{N}^X),$$

transforming latent variables  $Z \subset \mathcal{M}_Z \subset \mathbb{R}^n$  to the corresponding observed data  $X \subset \mathcal{M}_X \subset \mathbb{R}^N$ , with  $n < N$ , where  $\mathcal{M}_Z$  and  $\mathcal{M}_X$  are the manifold in the respective space. The objective of manifold learning is to find the inverse local homeomorphism

$$\Phi : \mathcal{G}(X, D^X, \mathcal{N}^X) \rightarrow \mathcal{G}(Z, D^Z, \mathcal{N}^Z).$$

**Cascade of local homeomorphisms.** Based on that the tangent space of a manifold is locally isomorphic to an Euclidean metric space, we could decompose a highly nonlinear  $\Phi$  into a cascade of  $L$  less nonlinear, locally isometric homeomorphisms  $\Phi = \phi^{(L)} \circ \dots \circ \phi^{(2)} \circ \phi^{(1)}$ . This leads to MLDL neural networks of the following form

$$\Phi : \mathcal{G}(X^{(0)}, D^{(0)}, \mathcal{N}^{(0)}) \xrightarrow{\phi^{(1)}} \mathcal{G}^1(X^{(1)}, D^{(1)}, \mathcal{N}^{(1)}) \xrightarrow{\phi^{(2)}} \dots \xrightarrow{\phi^{(L)}} \mathcal{G}^L(X^{(L)}, D^{(L)}, \mathcal{N}^{(L)}),$$

in which  $X^{(0)} = X$  is the input data,  $\phi^{(l)}$  the nonlinear transformation at layer  $l \in \{0, \dots, L\}$ ,  $X^{(l)} \subset \mathbb{R}^{N_l}$  the output of  $\phi^{(l)}$ ,  $\mathcal{N}^{(l)}$  the neighborhood system, and  $D^{(l)} = [d_l(x_i^{(l)}, x_j^{(l)})]$  the distance matrix given metric  $d_l$ . The layer-wise transformation can be written as

$$X^{(l+1)} = \phi^{(l)}(X^{(l)}, D^{(l)}, \mathcal{N}^{(l)} | W^{(l)}),$$

in which  $W^{(l)}$  is the weight matrix to be learned,  $D^{(l)}$  is used for locality restriction, and the product  $W^{(l)}X^{(l)}$  is followed by a nonlinear activation  $\sigma$ . Note that between any two layers  $l$  and  $l'$  is an effective compositional homeomorphism  $\phi^{(l,l')} : X^{(l)} \rightarrow X^{(l')}$ . We can define a quality metric for  $\Phi$  by a loss function of  $W$ .

For the manifold learning purpose, an ML encoder like the cascade gradually unfolds a nonlinear manifold  $\mathcal{M}_X$  into an embedding  $\mathcal{M}_Z$  in a latent space to best preserve the local geometric structure of  $\mathcal{M}_X$ . Given  $X^{(0)} = X$ , the  $\phi^{(l)}$ 's transform  $\mathcal{M}^{(l-1)}$  onto  $\mathcal{M}^{(l)} \subset \mathbb{R}^{N_l}$ , finally obtaining the embedding as  $Z = X^{(L)} \subset \mathcal{M}_Z \subset \mathbb{R}^n$ .

### 3 Markov-Lipschitz neural networks

In this section, we develop the key ideas of the MLDL framework for manifold learning and data generation. MLDL differs from other deep learning methods in that it imposes the prior constraint of locally isometric smoothness (LIS) via cross-layer links (orange-colored arcs and dashed lines in Fig. 1) and this helps preserve the local geometric structure of data and stabilize neural networks.

#### 3.1 Isometry and Lipschitz optimality

The core in MLDL is the imposition of the prior LIS constraint across-layers and encoding it into an MRF-Gibbs distribution. It requires that the overall homeomorphism  $\Phi : X \rightarrow Z$  (and moreover their layered components) should satisfy the LIS constraint; that is, distance metrics be preserved locally,  $d_X(x_i, x_j) = d_Z(\Phi(x_i), \Phi(x_j))$ , for  $j \in \mathcal{N}_i$ , as far as possible. Such a  $\Phi$  can be learned by minimizing the following loss

$$\mathcal{L}_{iso} = \left| d_X(x_i, x_j) - d_Z(\Phi(x_i), \Phi(x_j)) \right|. \quad (1)$$

$\mathcal{L}_{iso}$  measures the distortion in geometric distance and reaches the lower bound of zero when the isometry constraint is completely satisfied.  $\Phi$  is said to be locally Lipschitz if for all  $j \in \mathcal{N}_i$  there exists  $K > 0$  with

$$d_Z(\Phi(x_i), \Phi(x_j)) \leq K d_X(x_i, x_j).$$

A Lipschitz mapping or homeomorphism with a smaller  $K$  tends to generalize better [3, 1], be more robust to adversarial attacks [31, 8], and more stable in generative model learning [?, 25]. It is locally bi-Lipschitz if for all  $j \in \mathcal{N}_i$  there exists  $K \geq 1$  with

$$d_X(x_i, x_j)/K \leq d_Z(\Phi(x_i), \Phi(x_j)) \leq K d_X(x_i, x_j). \quad (2)$$

which is important for achieving invertible, bijective mappings between manifolds.

**Expected consequences.** We expect that imposing the LIS prior constraint and minimizing  $\mathcal{L}_{iso}$  should result in very good locally bi-Lipschitz continuity conditions, with  $K = 1$  being the best possible. This would not only preserve local geometric structure of data but also improve stability and robustness of resulting MLDL neural networks. Our extensive experiments on MLDL neural networks validate that resulting values of  $K$  are indeed much lower than those obtained with existing networks, proving that the use of the LIS prior constraint leads to decent Lipschitz conditions for stability and robustness.

#### 3.2 Markov-Lipschitz encoder

Based on the notion of local homeomorphisms and their cascade, we now introduce the idea of the cross-layer LIS prior constraint. We use the Markov-Lipschitz Encoder (ML-Enc) to illustrate how to use the LIS to optimize homeomorphic regularity for manifold learning and NLDR type of tasks.

**Cross-layer union of sample cliques.** The neighborhood systems  $\mathcal{N}$  at layers  $l$  and  $l'$  can be different due to the geometric deformations caused by the nonlinearity of  $\phi^{(l,l')} : X^{(l)} \rightarrow X^{(l')}$ . To cater for cross-layer neighborhood-based computation of LIS, we take the set union  $\mathcal{C}_2^{(l,l')} := \mathcal{C}_2^{(l)} \cup \mathcal{C}_2^{(l')}$ . Note that  $\#\mathcal{C}_2^{(l,l')} \leq \#\mathcal{C}_2^{(l)} + \#\mathcal{C}_2^{(l')}$  and the equality holds only when  $\mathcal{C}_2^{(l)} = \mathcal{C}_2^{(l')}$ . Clique set  $\mathcal{C}_3$  for triplet  $\{i, j, k\}$  and its cross-layer set union can also be defined as  $\mathcal{C}_3^{(l,l')} := \mathcal{C}_3^{(l)} \cup \mathcal{C}_3^{(l')}$  and used for angle-preserving to enhancing the distance-preserving constraints.

**Cross-layer LIS constraints.** The LIS constraint of Equ. (1) and (2) could be imposed across any two layers. Define the clique potential for cross-layer super-clique  $\lambda = (l, l') \in \Lambda$  for the network and data sample clique  $c = \{i, j\} \in \mathcal{C}_2^{(\lambda)}$  as

$$V_{\lambda,d}(\tilde{X}_c) = \left| d_l(x_i^{(l)}, x_j^{(l)}) - d_{l'}(x_i^{(l')}, x_j^{(l')}) \right|.$$

Summing the potentials up gives rise to the energy

$$\mathcal{L}_{iso}(W) = \sum_{\lambda \in \Lambda} \alpha^{(\lambda)} \sum_{c \in \mathcal{C}_2}^{\lambda} V_{\lambda,d}(\tilde{X}_c), \quad (3)$$

in which  $\alpha^{(\lambda)}$  are weights. Given the architecture, the transform  $\Phi$  is parameterized by  $W$ . Minimizing  $\mathcal{L}_{iso}(W)$  gives rise to the optimal solution for  $\Phi$ .

It is interesting to compare the LIS with the differential smoothness as defined by Equ. (3) and (4) in [14]. There, transformations in feedforward networks and residual networks are studied based on principles of Riemannian geometry. The differential smoothness assumes that vectors at successive layers are of the same dimensionality and cross-layer changes are infinitesimal. In MLDL, metrics between vectors, rather than the vectors themselves, are coped with and this allows arbitrary changes in the dimensionality, making the MLDL framework practically applicable.

**Cross-layer angular loss.** While the isometry is imposed on pairwise cliques  $\{i, j\}$  across-layers, a cross-layer angle-preserving constraint on triplet cliques of three points  $\{c = \{i, j, k\} \in \mathcal{C}_3^{(\lambda)}\}$  can be defined

$$V_{\lambda,A}(\tilde{X}_c) = \left| A(x_i^{(l)}, x_j^{(l)}, x_k^{(l)}) - A(x_i^{(l')}, x_j^{(l')}, x_k^{(l')}) \right|,$$

in which  $A(\cdot)$  is the angle function. The corresponding energy function is

$$\mathcal{L}_{ang}(W) = \sum_{\lambda \in \Lambda} \beta^{(\lambda)} \sum_{c \in \mathcal{C}_3}^{\lambda} V_{\lambda,A}(\tilde{X}_c), \quad (4)$$

in which  $\beta^{(\lambda)}$  are weights. The angle term is related to the isometry term but in a nonlinear way. We would like to evaluate its potential benefit.

**Homeomorphic regularity.** The isometric and angular losses as well are summed into  $\mathcal{L}_{reg}(W) = \mathcal{L}_{iso}(W) + \mathcal{L}_{ang}(W)$  measuring the geometric distortion and homeomorphic (ir)regularity. It is encoded as the energy in the corresponding prior Gibbs distribution  $p(\Phi|W)$ . While the LIS constraint is defined a priori, the loss  $\mathcal{L}_{reg}(W)$  is dependent on the data  $X$ . In future work, we will be investigating connections between this energy functions given  $X$  and the posterior distribution  $p(\Phi|X, W)$ .

**Push-Away loss.** This loss is introduced as an auxiliary cross-layer term to avoid deadlocks (knotting, bending) during the training. It is defined as

$$\mathcal{L}_{push}(W) = - \sum_{\lambda \in \Lambda} \sum_{c \notin \mathcal{C}_2^{(l)}} \pi[d_{l'}(x_i^{(l')}, x_j^{(l')}) < B] d_{l'}(x_i^{(l')}, x_j^{(l')}),$$

in which  $\pi[\cdot] \in \{0, 1\}$  is an indicator. This term encourages pairwise cliques that are non-neighbors,  $c = \{i, j\} \notin \mathcal{C}_2^{(l)}$ , at layer  $l$  but whose distance at layer  $l'$  is however smaller than a bound  $B$ , to push away from each other at layer  $l'$ . This term is imposed from the beginning of the training and as the training progresses, its influence is gradually decreased to zero. We find empirically that this continuation method significantly helps prevent the training from falling into a bad local optimum. We will investigate mechanisms behind in the future.

**ML-Enc loss function.** The ML-Enc learns an NLDR transformation  $\Phi : \mathbb{R}^N \rightarrow \mathbb{R}^n$  through manifold learning. The final objective function is the isometric loss, with the transit, auxiliary push-away loss added to help avoid falling into a bad minimum. Adding  $\mathcal{L}_{iso}(W)$  and the optional  $\mathcal{L}_{ang}(W)$  for optimizing homeomorphic regularity  $\mathcal{L}_{reg}(W) = \mathcal{L}_{iso}(W) + \mathcal{L}_{ang}(W)$  and the auxiliary  $\mathcal{L}_{push}(W)$ , we obtain the total lose for ML-Enc as

$$\mathcal{L}_{Enc}(W) = \mathcal{L}_{reg}(W) + \mu \mathcal{L}_{push}(W),$$

in which  $\mu$  gradually decreases from a starting value to 0.

### 3.3 Markov-Lipschitz AutoEncoder

The Markov-Lipschitz AutoEncoder (ML-AE) has two purposes: (1) helping regularize ML-Enc based manifold learning and (2) enabling manifold data generation. It is constructed by appending an ML decoder (ML-Dec) to ML-Enc in network structure and by adding reconstruction loss. The ML-Dec implements the inverse of ML-Enc and is entirely symmetric to the ML-Enc in its structure (see Fig. 1). In addition to the standard reconstruction loss  $\sum_{i=1}^M \|x_i^{(0)} - \hat{x}_i^{(0)}\|^2$  between the input layer (0) and the output layer (0'), the ML-AE makes a fuller use of the cross-layer LIS constraint in hope of achieving better reconstruction errors and the Lipschitz constant.

**Cross-layer constraints between encoder and decoder.** With some abuse of notations, we use  $\mathcal{S}'_L = \{L', \dots, 0'\}$  to denote the symmetric layers of the ML-Dec, with layer  $L' = L$  shared by the ML-Enc. Let  $\tilde{X}' = \{\hat{X}^{(0')}, \hat{X}^{(1')}, \dots, \hat{X}^{(L')}\}$ , with  $\hat{X} = \hat{X}^{(0')}$  as the output. A neighborhood system  $\mathcal{N}_{AE}$  and a set  $\Lambda_{AE}$  of pairwise super-cliques can be defined on  $\mathcal{S}_L \cup \mathcal{S}'_L$ .  $\tilde{X} \cup \tilde{X}'$  is an MRF on  $\mathcal{S}_L \cup \mathcal{S}'_L$  with respect to  $\mathcal{N}_{AE}$  if the Markovianity and the positivity conditions are satisfied.  $\Lambda_{AE}$  for the enhanced ML-AE is defined as follows: it includes  $\Lambda_L$  of the ML-Enc and the symmetrically mirrored counterpart of  $\Lambda_L$  for the ML-Dec; it further includes the super-cliques (links) between corresponding layers of ML-Enc and ML-Dec, shown in the dashed links in Fig. 1. Given  $\Lambda_{AE}$ , the isometric loss for the ML-AE,  $\mathcal{L}'_{iso}(W)$ , can be defined in a similar way to that for the ML-Enc in Equ. (3).

**ML-AE loss function.** Layer-wise reconstruction losses are summed up for each pair of the corresponding layers between ML-Enc and ML-Dec

$$\mathcal{L}_{rec}(W) = \sum_{l=0}^{L-1} \gamma_l \sum_{i=1}^M \|x_i^{(l)} - \hat{x}_i^{(l)}\|^2, \quad (5)$$

in which  $\gamma_l$  are weights. With the above preparation, we define the ML-AE loss as

$$\mathcal{L}_{AE}(W) = \mathcal{L}'_{iso}(W) + \mathcal{L}_{rec}(W) + \mu \mathcal{L}_{push}(W).$$

This loss differs from that of standard AE by  $\mathcal{L}'_{iso}$  and  $\mathcal{L}_{push}(W)$ .

## 4 Experiments

The purpose of the experiments is to evaluate the ML-Enc and ML-AE in their ability to preserve local geometry of manifolds and to achieve good stability and robustness in terms of relevant evaluation metrics.

**Data sets.** The Swiss Roll and S-Curve data, generated by the sklearn library [24], are used for the experiments. The data sets are normalized with the scaling factor of 1/20 for the Swiss Roll and 1/2 for the S-Curve. **Seven methods for manifold learning** are compared: ML-Enc (this paper), HILLE [9], MLLE and LTSA[33], ISOMAP [28], LLE [27] and t-SNE [21]; **Four autoencoder methods** are compared for manifold learning, reconstruction and data generation: ML-AE (this paper), AE [15], VAE [18], and TopoAE [23]. Due to the page limitation, the main body of the paper presents only main results with the Swiss Roll; more detailed results are presented in Appendix.

**Evaluation metrics** include the following. (1) Number of successes (**#Succ**) is the number of successes out of 10 solutions from random initialization in unfolding the manifold. (2) Local KL divergence (**L-KL**) measures the difference between distributions of local distances in the input and latent spaces. (3) Relative rank error (**RRE**) measures changes in neighbor ranking in the two spaces. (4) Trustworthiness (**Trust**) measures how well neighbors are preserved between the two spaces. (5) Locally geometric distortion (**LGD**) measures how much corresponding distances between neighboring points differ in two metric spaces. (6) Mean projection error (**MPE**) measures the "coplanarity" of 2D embeddings in a high-D space (in the following, the 3D layer before the 2D latent layer). (7) Minimum (**K-Min**) and (8) Maximum (**K-Max**) of local bi-Lipschitz constant in Equ.(2). (9) Mean reconstruction error (**MRE**) measures the difference between the input and output of autoencoders. Of the above, the MPE (or "coplanarity") and  $K$ -Min and  $K$ -Max are used for the first time as evaluation metrics for manifold learning. Their exact definitions are given in **Appendix A.1**. Every set of experiments is run 10 times, each with a data set generated using a random seed in  $\{0, 1, \dots, 9\}$ . Every final metric to be shown in performance tables is the average of the 10 results. When a run is unsuccessful in unfolding the input manifold data, the resulting averaged statistics of metrics are not very meaningful so the numbers will be shown in gray color in the following tables of evaluation metrics.

**The Euclidean distance metric** is used for all layers ( $d_l$ ); it is normalized as  $d'_l = d_l / \sqrt{n_l}$  for a space of dimensionality  $n_l$ . **The Neighborhood** is defined by the  $r$ -ball scheme with  $r = 0.23$ . **Push-away bound** is set to  $B = 3$ . **Minibatch size** is chosen according to the type and size of data. **Activation function:** LeakyReLU is used. **Continuation on  $\mu$ :**  $\mu$  starts from 0.8 and decreases linearly to the minimum 0 for epochs from 500 to 1000. **Epochs:** 3000 epochs are run for all results. The implementation is based on the PyTorch library running on Ubuntu 18.04 on NVIDIA v100 GPU.

### 4.1 ML-Enc for manifold Learning

The ML-Enc architecture in these set of experiments consists of 5 layers (3-100-100-100-3-2) with one cross-layer link  $\Lambda = (0, 5)$ , using  $\alpha^{(0,5)} = 1$  for  $\mathcal{L}_{iso}$ , and  $\beta^{(0,5)} = 0$  for  $\mathcal{L}_{ang}$ .

**Embedding quality.** Table 1 compares the ML-Enc with 6 other methods in 8 evaluation metrics, using the Swiss Roll (800 points) manifold data (the higher #Succ and Trust are, the better; the lower the other metrics, the better).

Results with the S-Curve are given in **Appendix A.2**. While the MPE is calculated at layer 4 (3D), the other metrics are calculated between the input and the latent layer. The results demonstrate that the ML-Enc outperforms all the other methods in all the evaluation metrics, particularly significant in terms of the isometry (LGD, RRE and Trust) and Lipschitz ( $K$ -Min and  $K$ -Max) related metrics. Visualizations of the learned embeddings are shown in **Appendix A.3**.

Table 1: Comparison of embedding quality for Swiss Roll (800 points)

	#Succ	L-KL	RRE	Trust	LGD	$K$ -Min	$K$ -Max	MPE
ML-Enc	<b>10</b>	<b>0.0184</b>	<b>0.000414</b>	<b>0.9999</b>	<b>0.00385</b>	<b>1.00</b>	<b>2.14</b>	<b>0.0262</b>
MLLE	6	0.1251	0.030702	0.9455	0.04534	7.37	238.74	0.1709
HLLE	6	0.1297	0.034619	0.9388	0.04542	7.44	218.38	0.0978
LTSA	6	0.1296	0.034933	0.9385	0.04542	7.44	215.93	0.0964
ISOMAP	6	0.0234	0.009650	0.9827	0.02376	1.11	34.35	0.0429
t-SNE	0	0.0450	0.006108	0.9987	3.40665	11.1	1097.62	0.1071
LLE	0	0.1775	0.014249	0.9753	0.04671	6.17	451.58	0.1400

**Robustness to sparsity and noise.** Table 2 evaluates the success rates of 5 manifold learning methods (t-SNE and LLE not included because they had zero success) in their ability to unfold the manifold and robustness to varying numbers of samples (700, 800, 1000, 1500, 2000) and standard deviation of noise  $\sigma = 0.05, 0.10, 0.15, 0.20, 0.25, 0.30$ . The corresponding evaluation metrics are provided in **Appendix A.4**. These two sets of experiments demonstrate that the ML-Enc achieves the highest success rate, the best performance metrics, and the best robustness to data sparsity and noise.

Table 2: Success rates with varying numbers of samples and noise levels

	#Samples					Noise level					
	700	800	1000	1500	2000	0.05	0.10	0.15	0.20	0.25	0.30
ML-Enc	<b>10</b>	<b>10</b>	<b>10</b>	<b>10</b>	<b>10</b>	<b>10</b>	<b>10</b>	<b>10</b>	<b>9</b>	<b>8</b>	<b>8</b>
MLLE	2	7	7	<b>10</b>	<b>10</b>	7	7	6	6	5	4
HLLE	2	6	7	<b>10</b>	<b>10</b>	7	7	6	6	5	3
LTSA	2	6	7	<b>10</b>	<b>10</b>	7	7	6	6	5	3
ISOMAP	2	6	7	<b>10</b>	<b>10</b>	7	7	6	6	5	4

**Generalization to unseen data.** The ML-Enc trained with 800 points can generalize to unseen data of the same manifold. First, 8000 test points of the Swiss Roll manifold are generated; then the manifold data are modified by removing respective points inside a shape of diamonds, square, pentagram or by making five-rings, creating 4 test sets. The trained ML-Enc is able to transform each test into the respective embedding in a way that the original shape is well preserved (see **Appendix A.5**). This means that the learned ML-Enc has a good ability to generalize to unseen data. In contrast, AE and VAE (and TopoAE) failed to unfold the data.

## 4.2 ML-AE for reconstruction and generation

This set of experiments compare the ML-AE with AE [15], VAE [18], and TopoAE [23], using the same architecture 3-100-100-100-3-2-3-100-100-100-100-3. The ML-AE uses one cross-layer link  $\Lambda = (0, 5)$  with cross-layer weights  $\alpha^{(0,5)} = 1$  for  $\mathcal{L}_{iso}$ ,  $\beta^{(0,5)} = 0$  for  $\mathcal{L}_{ang}$ , and  $\gamma_0 = \gamma_1 = \gamma_2 = \gamma_3 = \gamma_4 = 0.2$  for  $\mathcal{L}_{rec}$ .

**Manifold reconstruction.** The four autoencoders are trained with the Swiss Roll (800 points) data. However, only the ML-AE has successfully unfolded the Swiss Roll manifold. So, Table 3 provides the performance numbers for the ML-AE only while the others are moved to **Appendix A.6**. The MPE in the table is the average of the MPE's at layers 4 and 4' and the other metrics are calculated between the input and output layers of the AE's.

Table 3: Performance metrics for the ML-AE with Swiss Roll (800 points) data

	#Succ	L-KL	RRE	Trust	LGD	$K$ -Min	$K$ -Max	MPE	MRE
ML-AE	10	0.00165	0.00070	0.9998	0.00514	1.01	2.54	0.04309	0.01846

**Manifold data generation.** The ML-Dec part of the trained ML-AE can be used to generate new data of the learned manifold, mapping from random samples in the latent space to points in the higher-dimensional ambient space. Manifold data thus generated, shown in **Appendix A.7**, appear well placed.

### 4.3 Ablation study

This studies effects of the loss terms used in the ML-AE on the 9 performance metrics, calculated between corresponding layers of the encoder and decoder, with the Swiss Roll (800 points) data: (A) the isometric loss  $\mathcal{L}_{iso}$ , (B) the angular loss  $\mathcal{L}_{ang}$  and (C) the push-away loss  $\mathcal{L}_{push}$ . After analyzing the results in Table 4, we can conclude: (1) the isometric term (A) is the most important factor for achieving the results of excellence; (2) the push-away term (C), applied with decreasing weight and diminishing on convergence, helps unfold manifolds especially with challenging input; (3) the angular term (B) has little added value. Note, however, metric numbers for the unsuccessful cases do not make much sense for comparison.

Table 4: Ablation study of three loss items used in MLDL

	#Succ	L-KL	RRE	Trust	LGD	$K$ -Min	$K$ -Max	MPE	MRE
AC	<b>10</b>	<b>0.00165</b>	<b>0.00070</b>	<b>0.9998</b>	<b>0.00514</b>	<b>1.01</b>	<b>2.54</b>	0.04309	<b>0.01846</b>
ABC	<b>10</b>	0.00996	0.00156	0.9985	0.00557	<b>1.01</b>	6.93	<b>0.02387</b>	0.02513
AB	0	0.09315	0.09412	0.8346	0.03466	1.05	14.70	0.00911	0.24931
BC	0	0.05246	0.09052	0.8342	0.01640	1.02	14.99	0.00595	0.24960
A	0	0.07579	0.09127	0.8367	0.02776	1.05	11.34	0.00574	0.24499
B	0	0.07271	0.09559	0.8275	0.02536	1.06	22.47	0.01031	0.27439
C	0	0.06916	0.08457	0.8450	0.01896	1.05	125.69	0.00373	0.25894

## 5 Conclusions

The proposed MLDL framework imposes the cross-layer LIS prior constraint to optimize neural transformations in terms of local geometry preservation and network stability and robustness. Extensive experiments with manifold learning, reconstruction and generation consistently demonstrate that the MLDL networks (ML-Enc and ML-AE) well preserve local geometry for manifold learning and generation and achieve excellent local bi-Lipschitz constants for stability and robustness, advancing deep learning techniques. The main ideas of MLDL are general and effective enough, potentially applicable to a wide range of neural networks for improving representation learning and network stability and robustness.

## Acknowledgments

We would like to acknowledge funding support from the Westlake University and Bright Dream Joint Institute for Intelligent Robotics, and thank Zicheng Liu, Zhangyang Gao, Haitao Lin and Yiming Qiao for their assistance in processing experimental results.

## References

- [1] Cem Anil, James Lucas, and Roger Grosse. Sorting out lipschitz function approximation. *arXiv preprint arXiv:1811.05381*, 2018.



- [2] Maren Awiszus and Bodo Rosenhahn. Markov chain neural networks. In *The IEEE Conference on Computer Vision and Pattern Recognition (CVPR) Workshops*, June 2018.
- [3] Peter Bartlett, Dylan J. Foster, and Matus Telgarsky. Spectrally-normalized margin bounds for neural networks. *arXiv e-prints*, page arXiv:1706.08498, June 2017.
- [4] J. Besag. “Spatial interaction and the statistical analysis of lattice systems” (with discussions). *Journal of the Royal Statistical Society, Series B*, 36:192–236, 1974.
- [5] Michael M. Bronstein, Joan Bruna, Yann LeCun, Arthur Szlam, and Pierre Vandergheynst. Geometric Deep Learning: Going beyond Euclidean data. *IEEE Signal Processing Magazine*, 34(4):18–42, July 2017.
- [6] Chao Chen, Xiuyan Ni, Qinxun Bai, and Yusu Wang. Toporeg: A topological regularizer for classifiers. *CoRR*, abs/1806.10714, 2018.
- [7] Lisha Chen and Andreas Buja. Local multidimensional scaling for nonlinear dimension reduction, graph drawing, and proximity analysis. *Journal of the American Statistical Association*, 104(485):209–219, 2009.
- [8] Jeremy M Cohen, Elan Rosenfeld, and J. Zico Kolter. Certified Adversarial Robustness via Randomized Smoothing. *arXiv e-prints*, page arXiv:1902.02918, February 2019.
- [9] David L Donoho and Carrie Grimes. Hessian eigenmaps: Locally linear embedding techniques for high-dimensional data. *Proceedings of the National Academy of Sciences*, 100(10):5591–5596, 2003.
- [10] Michael Gashler, Dan Ventura, and Tony Martinez. Iterative non-linear dimensionality reduction with manifold sculpting. In J. C. Platt, D. Koller, Y. Singer, and S. T. Roweis, editors, *Advances in Neural Information Processing Systems 20*, pages 513–520. Curran Associates, Inc., 2008.
- [11] Stuart Geman and Donald Geman. “Stochastic relaxation, Gibbs distribution and the Bayesian restoration of images”. *IEEE Transactions on Pattern Analysis and Machine Intelligence*, 6(6):721–741, November 1984.
- [12] William L. Hamilton, Rex Ying, and Jure Leskovec. Inductive Representation Learning on Large Graphs. *arXiv e-prints*, page arXiv:1706.02216, June 2017.
- [13] J. M. Hammersley and P. Clifford. “Markov field on finite graphs and lattices”. unpublished, 1971.
- [14] Michael Hauser and Asok Ray. Principles of riemannian geometry in neural networks. In I. Guyon, U. V. Luxburg, S. Bengio, H. Wallach, R. Fergus, S. Vishwanathan, and R. Garnett, editors, *Advances in Neural Information Processing Systems 30*, pages 2807–2816. Curran Associates, Inc., 2017.
- [15] Geoffrey E Hinton and Ruslan R Salakhutdinov. Reducing the dimensionality of data with neural networks. *science*, 313(5786):504–507, 2006.
- [16] Christoph Hofer, Roland Kwitt, Marc Niethammer, and Andreas Uhl. Deep learning with topological signatures. In I. Guyon, U. V. Luxburg, S. Bengio, H. Wallach, R. Fergus, S. Vishwanathan, and R. Garnett, editors, *Advances in Neural Information Processing Systems 30*, pages 1634–1644. Curran Associates, Inc., 2017.
- [17] Di Jin, Ziyang Liu, Weihao Li, Dongxiao He, and Weixiong Zhang. Graph convolutional networks meet markov random fields: Semi-supervised community detection in attribute networks. In *Proceedings of the AAAI Conference on Artificial Intelligence*, volume 33, pages 152–159, 2019.
- [18] Diederik P Kingma and Max Welling. Auto-encoding variational bayes. *arXiv preprint arXiv:1312.6114*, 2013.
- [19] Fabian Latorre, Paul Rolland, and Volkan Chen-PMLR2019Cevher. Lipschitz constant estimation of neural networks via sparse polynomial optimization. In *International Conference on Learning Representations*, 2020.
- [20] Stan Z. Li. *Markov Random Field Modeling in Computer Vision*. Springer, 1995.
- [21] Laurens van der Maaten and Geoffrey Hinton. Visualizing data using t-sne. *Journal of machine learning research*, 9(Nov):2579–2605, 2008.
- [22] James McQueen, Marina Meila, and Dominique Joncas. Nearly isometric embedding by relaxation. In D. D. Lee, M. Sugiyama, U. V. Luxburg, I. Guyon, and R. Garnett, editors, *Advances in Neural Information Processing Systems 29*, pages 2631–2639. Curran Associates, Inc., 2016.
- [23] Michael Moor, Max Horn, Bastian Rieck, and Karsten Borgwardt. Topological autoencoders. *arXiv preprint arXiv:1906.00722*, 2019.
- [24] F. Pedregosa, G. Varoquaux, A. Gramfort, V. Michel, B. Thirion, O. Grisel, M. Blondel, P. Prettenhofer, R. Weiss, V. Dubourg, J. Vanderplas, A. Passos, D. Cournapeau, M. Brucher, M. Perrot, and E. Duchesnay. Scikit-learn: Machine learning in Python. *Journal of Machine Learning Research*, 12:2825–2830, 2011.
- [25] Guo-Jun Qi. Loss-sensitive generative adversarial networks on lipschitz densities. *International Journal of Computer Vision*, pages 1–23, 2019.

- [26] Meng Qu, Yoshua Bengio, and Jian Tang. GMNN: Graph Markov Neural Networks. *arXiv e-prints*, page arXiv:1905.06214, May 2019.
- [27] Sam T Roweis and Lawrence K Saul. Nonlinear dimensionality reduction by locally linear embedding. *science*, 290(5500):2323–2326, 2000.
- [28] Joshua B Tenenbaum, Vin De Silva, and John C Langford. A global geometric framework for nonlinear dimensionality reduction. *science*, 290(5500):2319–2323, 2000.
- [29] Aladin Virmaux and Kevin Scaman. Lipschitz regularity of deep neural networks: analysis and efficient estimation. In S. Bengio, H. Wallach, H. Larochelle, K. Grauman, N. Cesa-Bianchi, and R. Garnett, editors, *Advances in Neural Information Processing Systems 31*, pages 3835–3844. Curran Associates, Inc., 2018.
- [30] Larry Wasserman. Topological Data Analysis. *arXiv e-prints*, page arXiv:1609.08227, September 2016.
- [31] Tsui-Wei Weng, Huan Zhang, Pin-Yu Chen, Jinfeng Yi, Dong Su, Yupeng Gao, Cho-Jui Hsieh, and Luca Daniel. Evaluating the Robustness of Neural Networks: An Extreme Value Theory Approach. *arXiv e-prints*, page arXiv:1801.10578, January 2018.
- [32] Hao Wu, Andreas Mardt, Luca Pasquali, and Frank Noe. Deep generative markov state models. In *Advances in Neural Information Processing Systems*, pages 3975–3984, 2018.
- [33] Zhenyue Zhang and Jing Wang. Mlle: Modified locally linear embedding using multiple weights. In *Advances in Neural Information Processing systems*, pages 1593–1600, 2007.

## Appendix

### A.1 Definitions of performance metrics

The following notations are used in the definitions:

- $d_l(i, j)$ : the pairwise distance in space  $X^{(l)}$  (e.g. the input space  $X$ );
- $d_{l'}(i, j)$ : the pairwise distance in space  $X^{(l')}$  (e.g. the latent space  $Z$ );
- $\mathcal{N}_i^{k,(l)}$ : the set of indices to the  $k$ -nearest neighbor ( $k$ NN) of  $x_i^{(l)}$ ;
- $\mathcal{N}_i^{k,(l')}$ : the set of indices to the  $k$ NN of  $x_i^{(l')}$ ;
- $r_{(i,j)}$ : the rank of closeness of  $x_j^{(l)}$  to  $x_i^{(l)}$ ;
- $r'_{(i,j)}$ : the rank of closeness of  $x_j^{(l')}$  to  $x_i^{(l')}$ .

The 9 evaluation metrics are defined below:

- (1) **#Succ** is the number of times, out of 10 runs each with a random seed, where a manifold learning method has successfully unfolded the 3D manifold (the Swiss Roll or S-Curve) in the input to a 2D planar embedding without twists, tearing, or other defects.
- (2) **L-KL** (Local KL divergence) measures the discrepancy between distributions of local distances in two spaces, defined as (the locality being confined by  $\sigma$  which we choose to be  $\sigma = 0.01$ )

$$KL_\sigma = \sum_{\{i,j\} \in \mathcal{C}_2^{(l,l')}} u_{i,j}^\sigma \log \left( \frac{u_{i,j}^\sigma}{v_{i,j}^\sigma} \right),$$

where  $u_{i,j}^\sigma$  and  $v_{i,j}^\sigma$  are defined based on the distances for cliques  $\{i, j\} \in \mathcal{C}_2^{(l,l')}$

$$u_{i,j}^\sigma = \frac{\exp\left(-\frac{d_l(i,j)^2}{\sigma}\right)}{\sum_j \exp\left(-\frac{d_l(i,j)^2}{\sigma}\right)}, \quad v_{i,j}^\sigma = \frac{\exp\left(-\frac{d_{l'}(i,j)^2}{\sigma}\right)}{\sum_j \exp\left(-\frac{d_{l'}(i,j)^2}{\sigma}\right)}.$$

- (3) **RRE** (Relative rank change) measures the average of changes in neighbor ranking between two spaces ( $l'$  and  $l$ ):

$$RRE = \frac{1}{(k_2 - k_1 + 1)} \sum_{k=k_1}^{k_2} \{MR_{l \rightarrow l'}^k + MR_{l' \rightarrow l}^k\},$$

with  $k_1 = 4$ ,  $k_2 = 10$ , and

$$MR_{l' \rightarrow l}^k = \frac{1}{H_k} \sum_{i=1}^M \sum_{j \in \mathcal{N}_i^{k,(l)}} \left( \frac{|r(i, j) - r'(i, j)|}{r(i, j)} \right),$$

$$MR_{l \rightarrow l'}^k = \frac{1}{H_k} \sum_{i=1}^M \sum_{j \in \mathcal{N}_i^{k,(l')}} \left( \frac{|r(i, j) - r'(i, j)|}{r'(i, j)} \right),$$

in which  $H_k$  is the normalizing term

$$H_k = M \sum_{l=1}^k \frac{|M - 2l|}{l}.$$

- (4) **Trust** (Trustworthiness) measures how well neighboring relationships are preserved in two spaces:

$$Trust = \frac{1}{k_2 - k_1 + 1} \sum_{k=k_1}^{k_2} \left\{ 1 - \frac{2}{Mk(2M - 3k - 1)} \sum_{i=1}^M \sum_{j \in \mathcal{N}_i^{k, (l')}} (r(i, j) - k) \right\}.$$

with  $k_1 = 4, k_2 = 10$ .

- (5) **LGD** (Locally geometric distortion) measures how much corresponding distances between neighboring points differ in two metric spaces and is the primary metric for isometry, defined as (with  $k_1 = 4$ , and  $k_2 = 10$ ):

$$LGD = \sum_{k=k_1}^{k_2} \sqrt{\sum_i^M \frac{\sum_{j \in \mathcal{N}_i^{k, (l')}} (d_l(i, j) - d_{l'}(i, j))^2}{(k_2 - k_1 + 1)^2 M(\#\mathcal{N}_i)}}.$$

- (6) **MPE** (Mean projection error) measures the "coplanarity" of a set of 3D points  $X = \{x_1, \dots, x_M\}$  (in this work, the 3D layer before the final 2D latent layer). The least-squares 2D plane in the 3D space is fitted from the 3D points  $X$ . The 3D points  $X$  is projected onto the fitted planes as  $P = \{p_1, \dots, p_M\}$ . The MPE is defined as

$$MPE = \frac{1}{M} \sum_{i=1}^M \|x_i - p_i\|_2.$$

- (7)  **$K$ -min** is the minimum of the local bi-Lipschitz constant for the effective homeomorphism between any two layers  $l$  and  $l'$ , with respect to the given neighborhood system.
- (8)  **$K$ -max** is the maximum of the local bi-Lipschitz constant for the effective homeomorphism between any two layers  $l$  and  $l'$ , with respect to the given neighborhood system.

$$K_{\text{Min}} = \min_{i=1}^M \max_{j \in \mathcal{N}_i^{k, (l)}} K_{i,j},$$

$$K_{\text{Max}} = \max_{i=1}^M \max_{j \in \mathcal{N}_i^{k, (l)}} K_{i,j},$$

with  $k = 5$  and

$$K_{i,j} = \max \left\{ \frac{d_l(i, j)}{d_{l'}(i, j)}, \frac{d_{l'}(i, j)}{d_l(i, j)} \right\}.$$

- (9) **MRE** (Mean reconstruction error) measures the difference between the input and output of an autoencoder, as usually defined. More generally, an MRE may also be defined to measure the difference between a pair of corresponding data in the multi-layer encoder and decoder.

While the meanings of **MRE** and KL-Divergence are well known, those of the other metrics are explained as follows:

- **#Succ** is the primary metric measuring the success rate of unfolding a manifold. Without successful unfolding, the other metrics would not make sense. This metric is based on manual observation (see examples in A.9 at the end of this document).
- **Trust** and **RRE** both measure changes in neighboring relationships across-layers and also appear to be usable for indicating success/failure in unfolding manifolds. They are highly (inversely) correlated.
- **LGD** is the primary metric measuring the degree to which the LIS constraint is violated. However, it is unable to detect folding.
- **$K$ -min** and  **$K$ -max** are the key metrics of local bi-Lipschitz continuity, with  $K\text{-max} \geq K\text{-min} \geq 1$ . The closer to 1 they are, the better the network homeomorphism preserves the isometry, the more stable the network is in training and the more robust it is against adversarial attacks.
- **$K$ -max** can effectively identify the collapse in the latent space. In other words, if the model maps the input data together,  **$K$ -max** will become very huge. **L-KL** is not sensitive to collapse.

Every set of experiments is run 10 times, each with a data set generated using a random seed in  $\{0, 1, \dots, 9\}$ . Every final metric shown is the average of the 10 results. When a run is unsuccessful in unfolding the input manifold data, the resulting averaged statistics of metrics are not very meaningful so the numbers will be shown in **gray color** in the following tables of evaluation metrics.

## A.2 ML-Enc manifold learning with S-Curve

The table below compares the ML-Enc with other algorithms in the 8 evaluation metrics for the S-Curve. The ML-Enc performs the best for all but MPE. Note, however, that t-SNE and LLE failed to unfold the manifold hence their results should be considered as invalid even if t-SNE achieved the lowest MPE value due to its collapsing to a small cluster. Because LLE and t-SNE have zero success rate, their metrics do not make sense hence not compared in the table. The results show that ML-Enc performs significantly better than the others for all the metrics except for MPE.

Comparison in embedding quality for S-Curve (800 points)								
	#Succ	L-KL	RRE	Trust	LGD	$K$ -min	$K$ -max	MPE
ML-Enc	<b>10</b>	<b>0.00718</b>	<b>0.000107</b>	<b>0.999985</b>	<b>0.000857</b>	<b>1.0025</b>	<b>1.62</b>	0.0818
MLLE	<b>10</b>	0.00931	0.008893	0.989943	0.045243	7.2454	32.43	0.1722
HLLE	<b>10</b>	0.00971	0.008866	0.990005	0.045243	7.2341	31.69	<b>0.0804</b>
LTSA	<b>10</b>	0.00971	0.008866	0.990005	0.045243	7.2341	31.69	0.0948
ISOMAP	<b>10</b>	0.00931	0.001762	0.999233	0.023359	1.1148	13.36	0.0173
LLE	0	0.05462	0.008055	0.989728	0.046917	8.4081	143.31	0.1445
t-SNE	0	0.01486	0.002071	0.999124	1.36791	14.6310	311.24	0.0412

## A.3 Visualization of ML-Enc manifold learning

The following show visualization of ML-Enc manifold and embedding learning results for 10 Swiss Roll and 10 S-Curve datasets. Such datasets are generated with a random seed in  $\{0, 1, \dots, 9\}$ . (20 such figures were produced so we decided to move them to A.9 at the end of this document.)

## A.4 Robustness to sparsity and noise

The table below shows evaluation metric numbers for varying numbers (densities) of training data points and noise levels, with the Swiss Roll (800 points) data. Here, four metrics, **Trust**, **LGD**,  $K$ -**min** and  $K$ -**max**, are selected to compare ML-Enc with others.

The results for different sample sizes are presented in the tables below.

**Trust with different sample sizes (given noise level = 0.0)**

	700	800	1000	1500	2000
ML-Enc	<b>0.9984</b>	<b>0.9999</b>	0.9859	<b>0.9999</b>	<b>0.9999</b>
MLLE	0.9079	0.9457	0.9646	0.9948	0.9960
HLLE	0.8984	0.9389	0.9587	0.9948	0.9962
LTSA	0.8983	0.9386	0.9586	0.9948	0.9962
ISOMAP	0.9662	0.9828	<b>0.9943</b>	0.9996	0.9997

**LGD with different sample sizes (given noise level = 0.0)**

	700	800	1000	1500	2000
ML-Enc	<b>0.0167</b>	<b>0.0040</b>	<b>0.0048</b>	<b>0.0016</b>	<b>0.0016</b>
MLLE	0.0480	0.0453	0.0407	0.0335	0.0293
HLLE	0.0483	0.0454	0.0408	0.0335	0.0293
LTSA	0.0483	0.0454	0.0408	0.0335	0.0293
ISOMAP	0.0261	0.0238	0.0208	0.0161	0.0139

**$K$ -min with different sample sizes (given noise level = 0.0)**

	700	800	1000	1500	2000
ML-Enc	<b>1.0059</b>	<b>1.0049</b>	<b>1.0167</b>	<b>1.0070</b>	<b>1.0063</b>
MLLE	6.4093	7.3723	8.5129	10.150	50.581
HLLE	6.7227	7.4430	8.4837	10.149	48.563
LTSA	6.7226	7.4428	8.4848	10.149	48.526
ISOMAP	1.1069	1.1075	1.1026	1.0968	8.3342

***K*-max with different sample sizes (given noise level = 0.0)**

	700	800	1000	1500	2000
ML-Enc	<b>2.9917</b>	<b>1.7239</b>	<b>18.306</b>	<b>1.9931</b>	<b>2.1216</b>
MLLE	360.03	240.62	442.48	43.901	50.581
HLLE	326.59	216.43	301.56	42.356	48.563
LTSA	314.81	215.84	296.37	42.358	48.526
ISOMAP	31.299	34.354	27.030	13.247	8.3342

The results for different noise levels are presented in the tables below.

**Trust with different noise levels (given #Samples = 800)**

	0.05	0.1	0.15	0.2	0.25	0.30
ML-Enc	<b>0.9998</b>	<b>0.9997</b>	<b>0.9999</b>	<b>0.9999</b>	<b>0.9858</b>	<b>0.9961</b>
MLLE	0.9614	0.9618	0.9406	0.9365	0.9339	0.9198
HLLE	0.9261	0.9265	0.9098	0.9121	0.9020	0.9121
LTSA	0.9261	0.9265	0.9098	0.9120	0.9020	0.9121
ISOMAP	0.9871	0.9873	0.9846	0.9849	0.9835	0.9808

**LGD with different noise levels (given #Samples = 800)**

	0.05	0.1	0.15	0.2	0.25	0.30
ML-Enc	<b>0.0045</b>	<b>0.0046</b>	<b>0.0046</b>	<b>0.0056</b>	<b>0.0060</b>	<b>0.0063</b>
MLLE	0.0454	0.0455	0.0457	0.0460	0.0465	0.0469
HLLE	0.0456	0.0457	0.0460	0.0464	0.0472	0.0473
LTSA	0.0461	0.0462	0.0461	0.0464	0.0468	0.0473
ISOMAP	0.0234	0.0234	0.0238	0.0239	0.0239	0.0242

***K*-min with different noise levels (given #Samples = 800)**

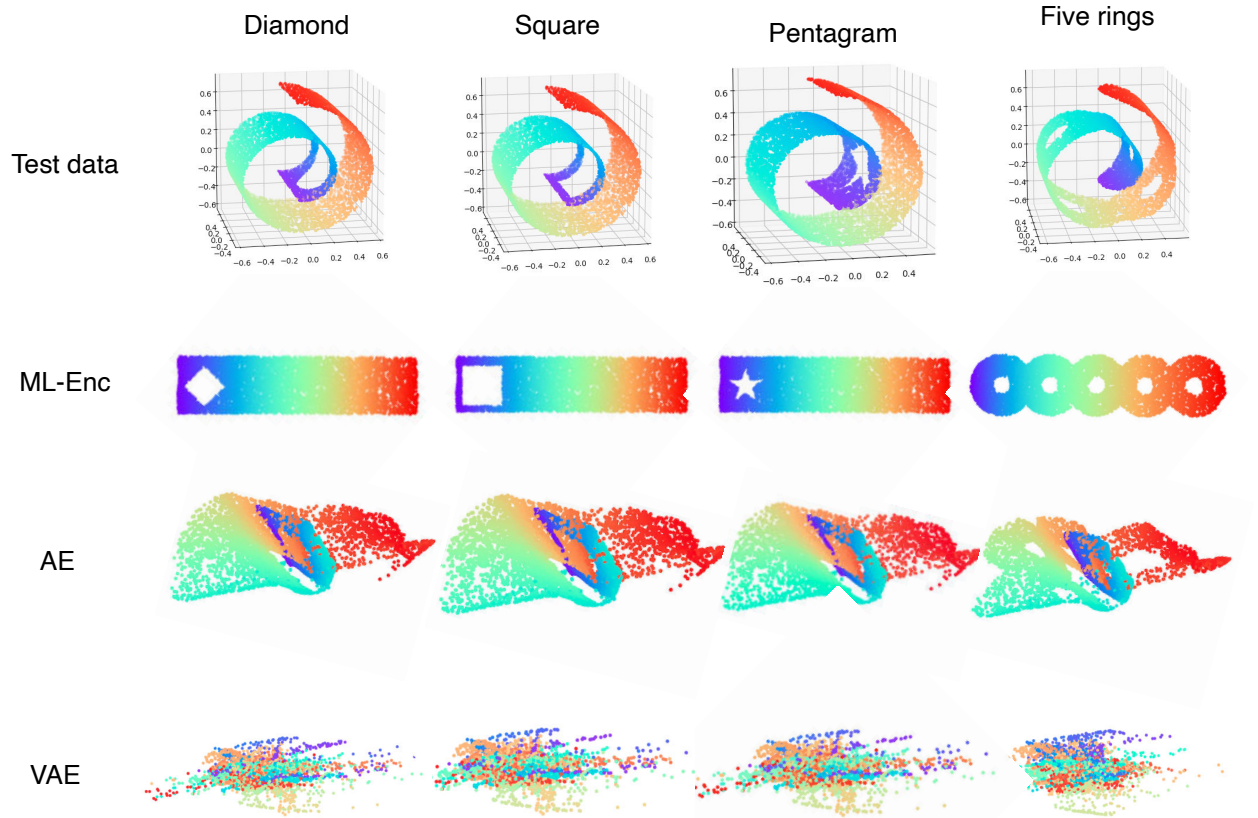
	0.05	0.1	0.15	0.2	0.25	0.30
ML-Enc	<b>1.0059</b>	<b>1.0056</b>	<b>1.0061</b>	<b>1.0062</b>	<b>1.0095</b>	<b>1.0114</b>
MLLE	7.5231	7.7358	7.6939	7.7791	7.7998	7.8526
HLLE	6.9776	7.0187	6.9877	7.2334	8.0168	8.3280
LTSA	7.6919	7.8743	7.4068	7.2687	7.4794	8.3280
ISOMAP	1.1140	1.1144	1.1257	1.1173	1.1042	1.0971

***K*-max with different noise levels (given #Samples = 800)**

	0.05	0.1	0.15	0.2	0.25	0.30
ML-Enc	<b>4.1507</b>	<b>5.4509</b>	<b>5.3142</b>	<b>6.0980</b>	<b>7.6605</b>	<b>14.523</b>
MLLE	304.80	181.17	256.56	416.28	272.59	299.81
HLLE	508.93	898.31	5997.3	8221.0	1162.0	714.14
LTSA	508.93	898.31	5997.3	8221.0	1162.0	714.14
ISOMAP	25.495	16.392	17.716	25.383	35.144	41.422

## A.5 Generalization to unseen data

The figure below demonstrates that a learned ML-Enc can generalize well to unseen data in unfolding a modified version of the same manifold to the corresponding version of embedding. The ML-Enc model is trained with a Swiss Roll (800 points) dataset. The test is done as follows: First, a set of 8000 points of the Swiss Roll manifold are generated; the data set is modified by removing, from the generated 8000 points of the manifold, the shape of a diamonds, square, pentagram or five-ring, respectively, creating 4 test sets. Each point of a test set is transformed independently by the trained ML-Enc to obtain an embedding. We can see from each of the resulting embeddings that the unseen manifold data sets are well unfolded by the ML-Enc and the removed shapes are kept very well, illustrating that the learned ML-Enc has a good ability to generalize to unseen data. Since LLE-based, LTSA and ISOMAP algorithms do not possess such a generalization ability, the ML-Enc is compared with the encoder parts of the AE based algorithms. Unfortunately, AE and VAE failed altogether for the Swiss Roll data sets.



## A.6 ML-AE for manifold learning and reconstruction

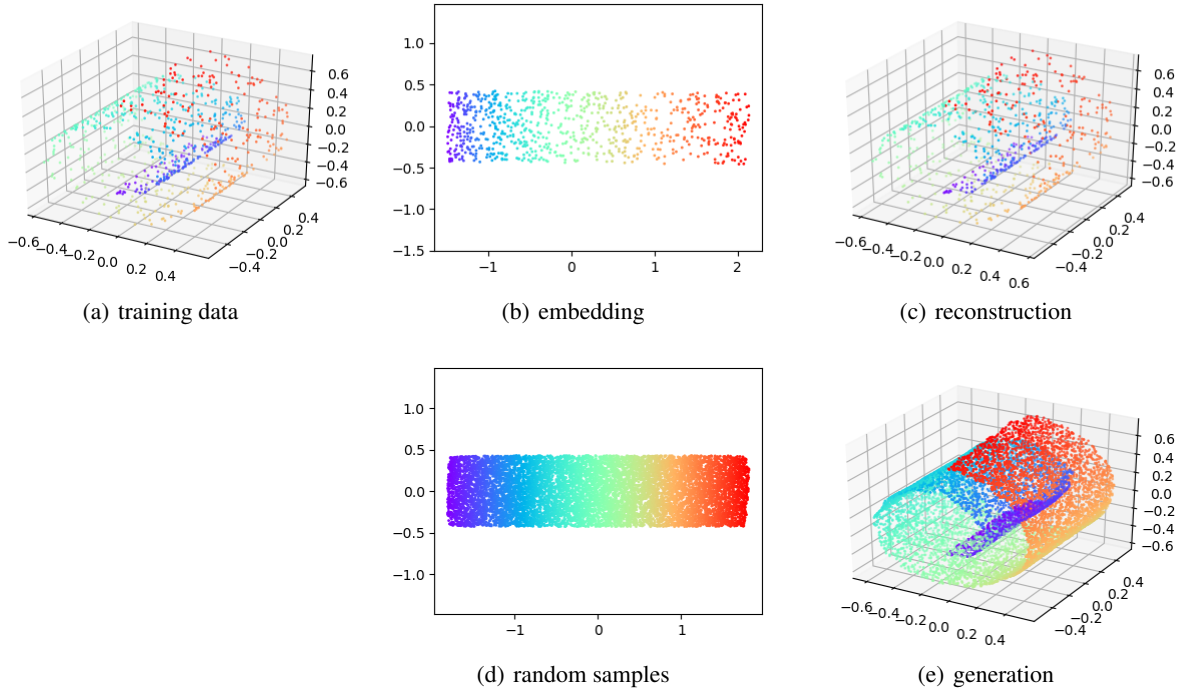
The following shows the complete Table 3 in Section 4.2 of the main text, comparing the 9 quality metrics (all being the averages of 10 runs), including the mean reconstruction error (MRE), for the 4 autoencoders with the Swiss Roll (800 points) data. While the other 3 autoencoders fail to unfold the manifold data sets (hence their metrics do not make much sense), the ML-AE produces good quality results especially in terms of the isometry and Lipschitz related metrics. The resulting metrics also suggest that  $K$ -max could be used as an indicator of success/failure in manifold unfolding.

**Table 3. Performance metrics of four autoencoders with the Swiss Roll (800 points) data**

	#Succ	L-KL	RRE	Trust	LGD	$K$ -min	$K$ -max	MPE	MRE
ML-AE	<b>10</b>	<b>0.00165</b>	<b>0.00070</b>	<b>0.9998</b>	<b>0.00514</b>	<b>1.01</b>	<b>2.54</b>	<b>0.04309</b>	<b>0.01846</b>
AE	0	0.11537	0.13589	0.7742	0.03069	1.82	5985.74	0.01519	0.40685
VAE	0	0.23253	0.49784	0.5053	0.04000	1.49	5290.55	0.01977	0.78104
TopoAE	0	0.05793	0.04891	0.9265	0.09651	1.10	228.11	0.12049	0.56013

## A.7 ML-AE for manifold data generation

The figure below shows manifold data reconstruction and generation using ML-AE, for which cases AE and VAE all failed in learning to unfold. In the learning phase, the ML-AE performs manifold learning for NLDR and then reconstruction, taking (a) the training data in the ambient space as input, output embedding (b) in the learned latent space, and then reconstruct back (c) in the ambient data space. In the generation phase, the ML-Dec takes as random input samples (d) in the latent space, and maps the samples to the manifold (e) in the ambient data space.



## A.8 More ablation for ML-AE loss terms

The ablation in Table 4 of Section 4.3 compares three loss terms used in the ML-AE: (A) the isometric loss  $\mathcal{L}_{iso}$ , (B) the angular loss  $\mathcal{L}_{ang}$  and (C) the push-away loss  $\mathcal{L}_{push}$ . There, the 9 performance metrics are calculated between the input and output layers of the ML-AE.

Here, we provide three more sets of ablation experiments. The first set compares the effects of the three terms in terms of the 9 metrics but which are calculated between the input and latent layers instead. The conclusion is similar (note



that for the models failed to unfold the manifold (where #Succ=0), the "best" metric numbers are not meaningful): (1) the isometric term (A) leads to  $K$ -min of 1.0 and is the most important for achieving the results of excellence; (2) the push-away term (C), applied with decreasing weight and diminishing on convergence, helps unfold manifolds especially with challenging input; (3) the angular term (B) has little added value. Overall, the "AC" combination is the best algorithm of all.

**Ablation study of three loss items used in ML-AE (metrics between input and latent layers)**

	#Succ	L-KL	RRE	Trust	LGD	$K$ -min	$K$ -max	MPE
AC	<b>10</b>	0.01842	<b>0.00041</b>	<b>0.9999</b>	<b>0.00386</b>	<b>1.00</b>	<b>2.15</b>	0.04309
ABC	<b>10</b>	<b>0.01823</b>	0.00143	0.9981	0.00425	<b>1.00</b>	4.92	<b>0.02388</b>
AB	0	0.06672	0.09701	0.8173	0.00414	1.00	7.19	0.00911
BC	0	0.05276	0.09071	0.8308	5.17885	91.49	291.84	0.00596
A	0	0.06257	0.09208	0.8271	0.00434	1.00	5.76	0.00574
B	0	0.05657	0.09675	0.8179	0.04608	26.52	469.63	0.01031
C	0	0.05213	0.09407	0.8303	27.76862	177.41	1089.54	0.00374

In the second set, we provide ablation experiments with different **cross-layer weight schemes for the ML-Enc**, based on the 5-layer network architecture (3-100-100-100-3-2) presented in Section 4.1. The following 6 different cross-layer weight schemes (nonzero  $\alpha$  weights in  $\mathcal{L}_{iso}$ ) are evaluated:

M1:  $\alpha^{(0,5)} = 1$  (between the input and latent layers only);

M2:  $\alpha^{(0,1)} = \frac{2}{30}, \alpha^{(1,2)} = \frac{4}{30}, \alpha^{(2,3)} = \frac{6}{30}, \alpha^{(3,4)} = \frac{8}{30}, \alpha^{(4,5)} = \frac{10}{30}$  (between each pair of adjacent layers, the weight increasing as the other layer goes deeper);

M3:  $\alpha^{(1,5)} = \frac{2}{30}, \alpha^{(2,5)} = \frac{4}{30}, \alpha^{(3,5)} = \frac{6}{30}, \alpha^{(4,5)} = \frac{8}{30}, \alpha^{(0,5)} = \frac{10}{30}$  (between the latent layer and each of the other layers, the weight increasing as the other layer goes deeper);

M4:  $\alpha^{(0,1)} = \frac{2}{30}, \alpha^{(0,2)} = \frac{4}{30}, \alpha^{(0,3)} = \frac{6}{30}, \alpha^{(0,4)} = \frac{8}{30}, \alpha^{(0,5)} = \frac{10}{30}$  (between the input layer and each of the other layers, the weight increasing as the other layer goes deeper).

M5:  $\alpha^{(0,1)} = \frac{1}{5}, \alpha^{(0,2)} = \frac{1}{5}, \alpha^{(0,3)} = \frac{1}{5}, \alpha^{(0,4)} = \frac{1}{5}, \alpha^{(0,5)} = \frac{1}{5}$  (between the input layer and each of the other layers, the weight being equal for all layers).

M6:  $\alpha^{(0,1)} = \frac{10}{30}, \alpha^{(0,2)} = \frac{8}{30}, \alpha^{(0,3)} = \frac{6}{30}, \alpha^{(0,4)} = \frac{4}{30}, \alpha^{(0,5)} = \frac{2}{30}$  (between the input layer and each of the other layers, the weight decreasing as the other layer goes deeper).

We are interested in evaluating the ML-Enc in its ability to preserve the local geometry structure not only at the latent layer, but also at intermediate layers. To see this aspect, we provide the metrics calculated between layer  $l = 0$  and layer  $l' \in \{1, 3, 5\}$ . The ablation results are shown in the table below. Schemes M1 and M4 have 100% success rate for the 10 runs, M5 and M6 have some successes whereas M2 and M3 have zero. Of M1 and M4, the latter seems better overall.

Evaluation metrics with different cross-layer schemes for ML-Enc									
$l-l'$	Method	#Succ	L-KL	RRE	Trust	LGD	$K$ -min	$K$ -max	MPE
0-1	M1	<b>10</b>	0.0026	0.000792	0.9997	0.03081	2.29	3.29	0.0262
	M2	0	0.0062	0.001156	0.9994	0.02981	2.06	3.45	0.0068
	M3	0	0.0038	0.001781	0.9989	0.02761	1.86	3.39	0.0093
	M4	<b>10</b>	<b>0.0011</b>	<b>0.000555</b>	<b>0.9998</b>	<b>0.01494</b>	<b>1.31</b>	<b>1.72</b>	<b>0.0135</b>
	M5	5	0.0006	0.000220	0.9999	0.00199	1.00	1.18	0.0576
	M6	2	0.0003	0.000084	0.9999	0.00081	1.00	1.08	0.0566
0-3	M1	<b>10</b>	0.0235	0.001534	0.9992	0.03541	2.28	5.98	0.0262
	M2	0	0.0667	0.047127	0.9021	0.03642	1.98	43.83	0.0068
	M3	0	0.0292	0.053970	0.8957	0.02235	1.09	49.98	0.0093
	M4	<b>10</b>	<b>0.0135</b>	<b>0.000516</b>	<b>0.9999</b>	<b>0.00443</b>	<b>1.00</b>	<b>1.57</b>	<b>0.0135</b>
	M5	5	0.0024	0.000182	0.9998	0.00110	1.00	1.14	0.0576
	M6	2	0.0031	0.000216	0.9997	0.00100	1.00	1.14	0.0566
0-5	M1	<b>10</b>	<b>0.0184</b>	<b>0.000414</b>	<b>0.9999</b>	<b>0.00385</b>	<b>1.00</b>	2.14	0.0262
	M2	0	0.0655	0.102837	0.8201	0.03631	1.71	1152.42	0.0068
	M3	0	0.0488	0.105081	0.8202	0.02166	1.09	994.12	0.0093
	M4	<b>10</b>	<b>0.0184</b>	<b>0.000440</b>	<b>0.9999</b>	<b>0.00400</b>	<b>1.00</b>	<b>1.73</b>	<b>0.0135</b>
	M5	5	0.0327	0.022078	0.9591	0.00630	1.01	3.68	0.0576
	M6	2	0.0454	0.030612	0.9430	0.01321	1.05	8.13	0.0566

In the third set, we provide ablation experiments with different **corresponding-layer weight schemes for the ML-AE**, based on the ML-AE architecture (3-100-100-100-3-2-3-100-100-100-100-3) presented in Section 4.3 where the LIS is imposed between layers 0 and 5 with  $\alpha^{(0,5)} = 1$  and all  $\gamma^{(l,l')} = 0.2$ . A corresponding-layer scheme is determined by nonzero  $\alpha$  weights in  $\mathcal{L}_{iso}$  between the corresponding layers in the ML-Enc and ML-Dec. The following 4 weight schemes are evaluated:

M7:  $\alpha^{(0,5)} = 1$  (No LIS constraints between corresponding-layers, as baseline);

M8:  $\alpha^{(0,5)} = 1, \alpha^{(0,0')} = \frac{2}{30}, \alpha^{(1,1')} = \frac{4}{30}, \alpha^{(2,2')} = \frac{6}{30}, \alpha^{(3,3')} = \frac{8}{30}, \alpha^{(4,4')} = \frac{10}{30}$  (the corresponding-layer weight for the LIS constraint increases as the layer number becomes bigger);

M9:  $\alpha^{(0,5)} = 1, \alpha^{(0,0')} = \frac{1}{5}, \alpha^{(1,1')} = \frac{1}{5}, \alpha^{(2,2')} = \frac{1}{5}, \alpha^{(3,3')} = \frac{1}{5}, \alpha^{(4,4')} = \frac{1}{5}$  (all the corresponding-layer weights for the LIS constraint are equal);

M10:  $\alpha^{(0,5)} = 1, \alpha^{(0,0')} = \frac{10}{30}, \alpha^{(1,1')} = \frac{8}{30}, \alpha^{(2,2')} = \frac{6}{30}, \alpha^{(3,3')} = \frac{4}{30}, \alpha^{(4,4')} = \frac{2}{30}$  (the corresponding-layer weight for the LIS constraint decreases as the layer number becomes bigger).

The ablation results are shown in the table below, where the metric numbers are calculated between layers  $l = 0$  and  $l' = 0'$ :

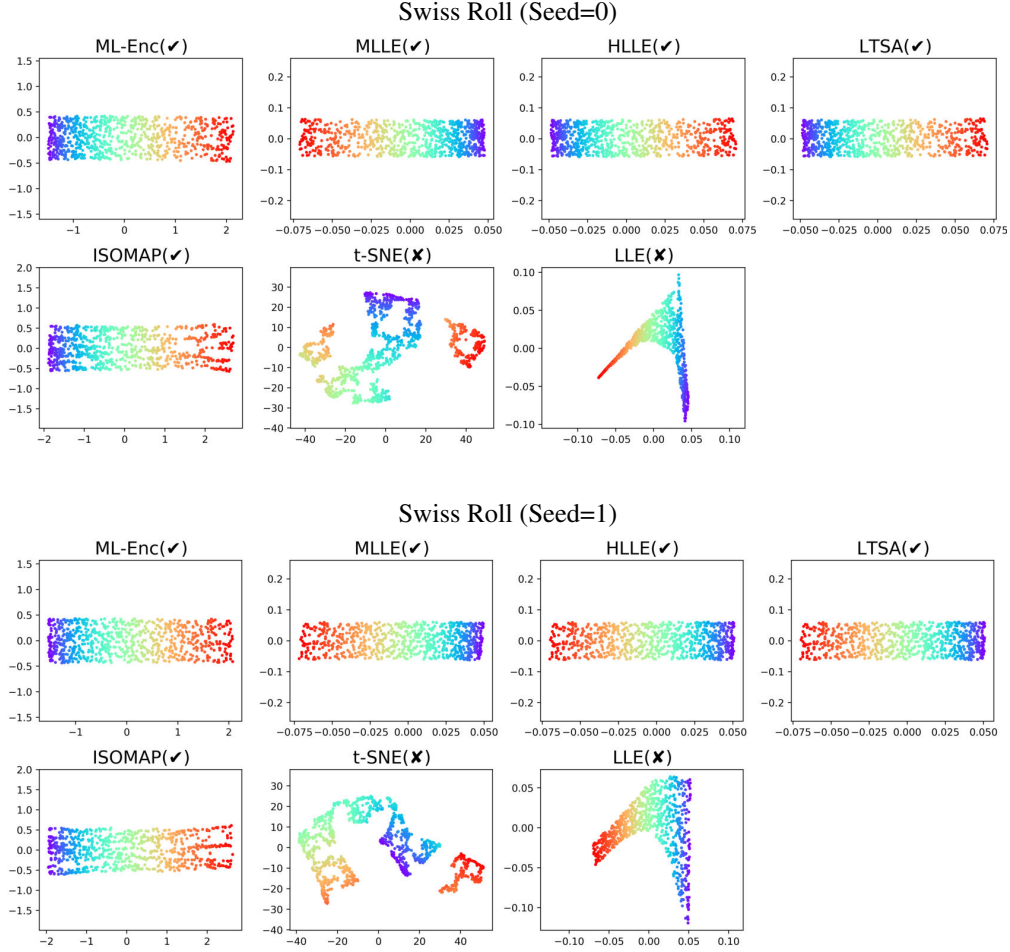
Evaluation metrics with different corresponding-layer schemes for ML-AE									
	#Succ	L-KL	RRE	Trust	LGD	$K$ -min	$K$ -max	MPE	MRE
M7	<b>10</b>	0.00165	0.00070	<b>0.9998</b>	0.00514	<b>1.017</b>	2.540	0.04309	0.01846
M8	<b>10</b>	0.00142	0.00065	<b>0.9998</b>	0.00480	<b>1.017</b>	<b>2.324</b>	0.04288	0.01810
M9	<b>10</b>	0.00168	0.00070	<b>0.9998</b>	0.00520	1.018	2.543	0.04279	0.01788
M10	<b>10</b>	<b>0.00121</b>	<b>0.00063</b>	<b>0.9998</b>	<b>0.00459</b>	<b>1.017</b>	2.377	<b>0.04269</b>	<b>0.01762</b>

The results demonstrate that M10 outperforms the other three schemes in all metrics except for one  $K$ -max. When compared with incremental and equal weight scheme (M8 and M9), decreasing the corresponding-layer weight for the LIS constraint as the layer number becomes bigger can result in the greater performance gain, since the closer the data is to the input layer in the Encoder, the more authentic and reliable it is.

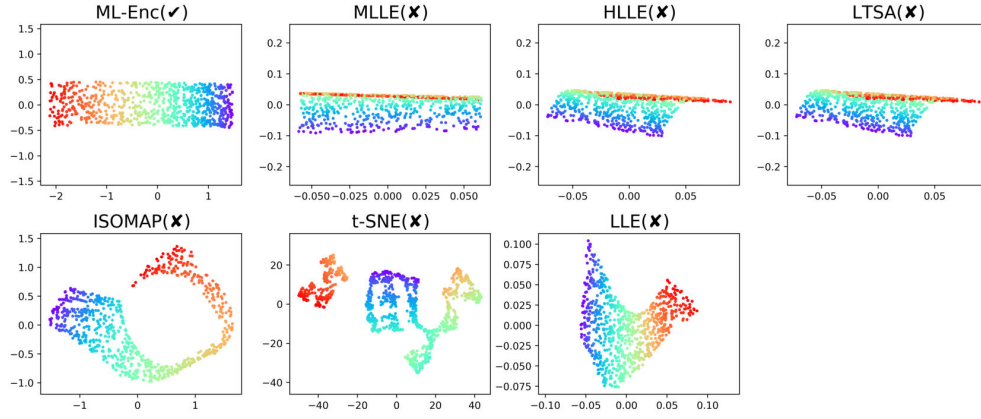
The ablation study shows that the use of the LIS constraint in MLDL has accomplished its promises and suggests further investigation into automatic learning of optimal links and weights for the LIS.

### A.9 Comparing manifold learning results by visualization

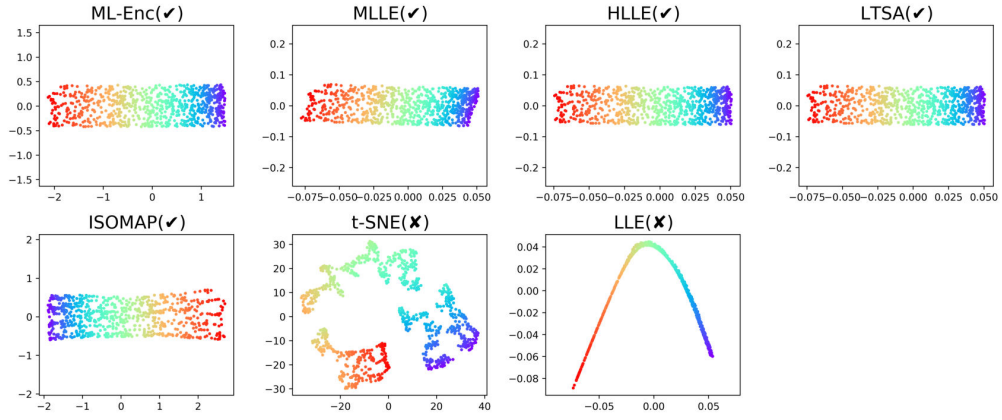
The following show visualization of ML-Enc manifold learning results for 10 Swiss Roll and 10 S-Curve datasets. Such datasets are generated with a random seed in  $\{0, 1, \dots, 9\}$ . In these figures, a symbol  $\checkmark$  or  $\times$  represents a success or failure in unfolding the manifold. From these results, we can see that the ML-Enc not only has the highest success rate, but also best maintains the true aspect ratio.



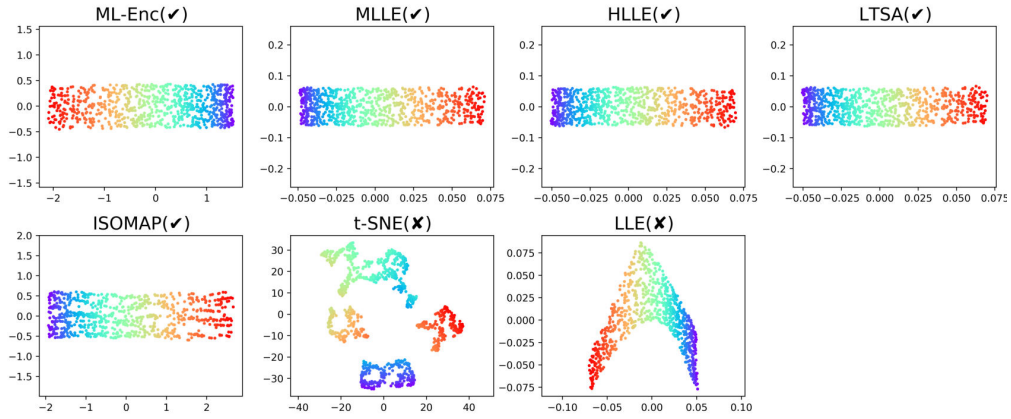
Swiss Roll (Seed=2)



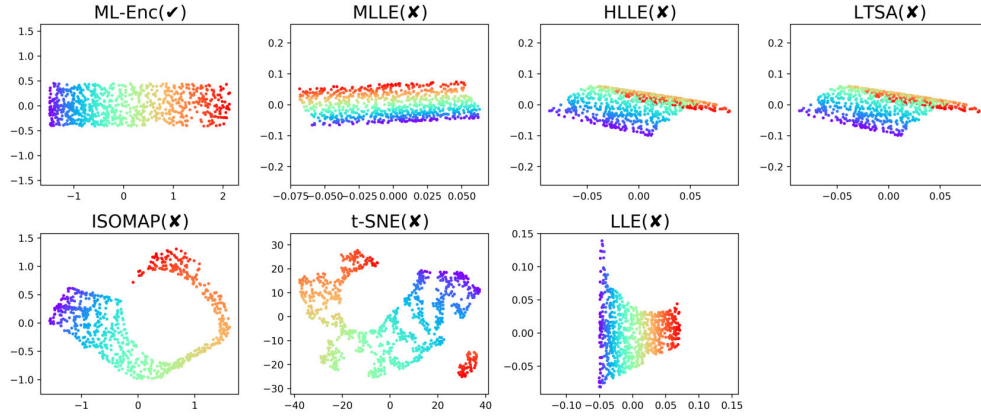
Swiss Roll (Seed=3)



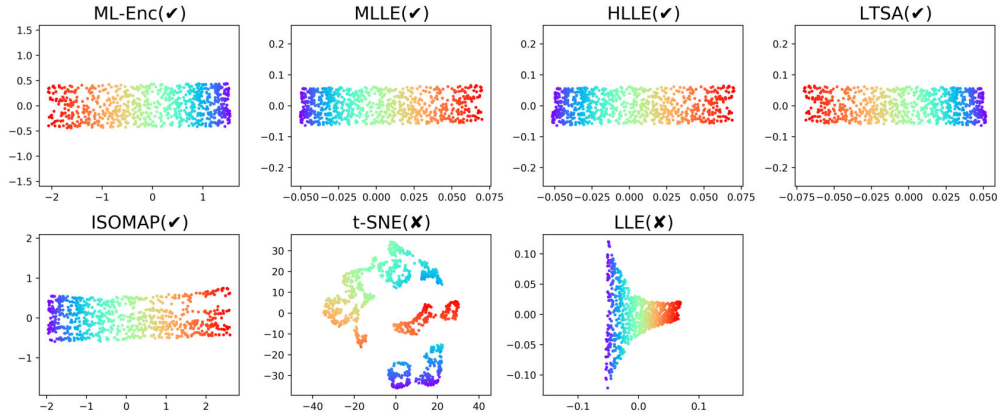
Swiss Roll (Seed=4)



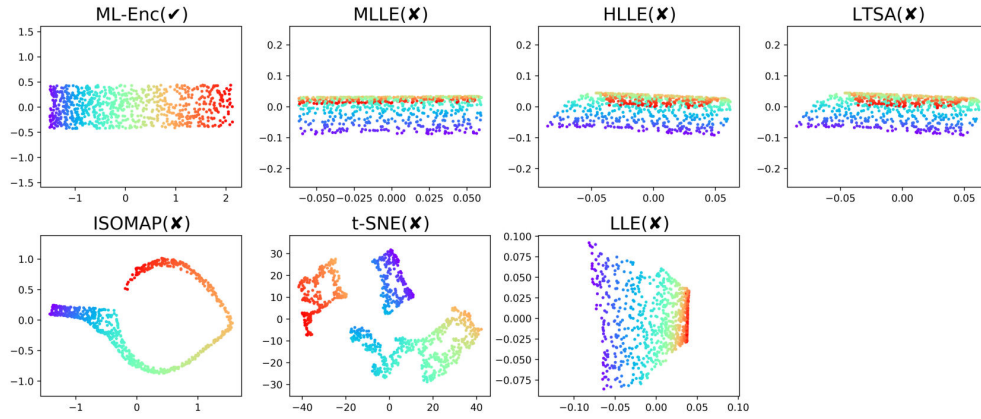
Swiss Roll (Seed=5)



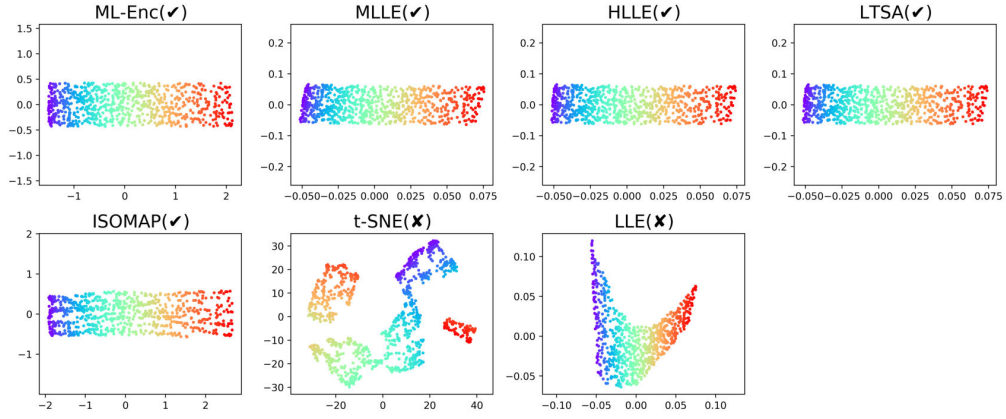
Swiss Roll (Seed=6)



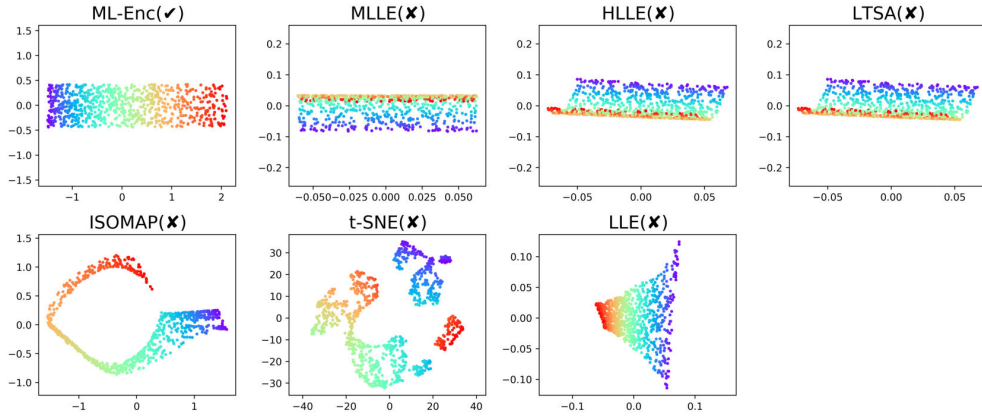
Swiss Roll (Seed=7)



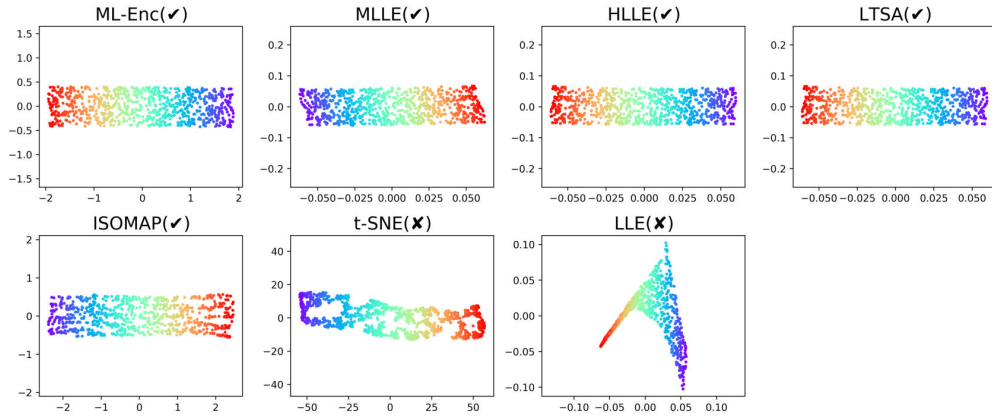
Swiss Roll (Seed=8)



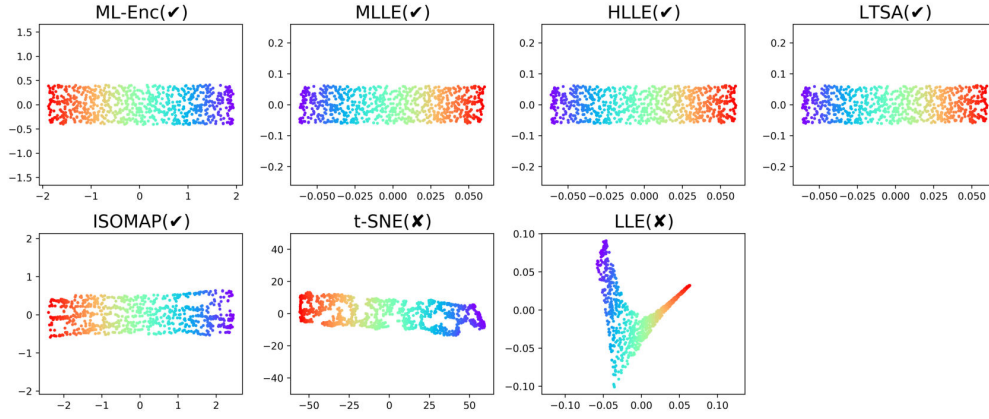
Swiss Roll (Seed=9)



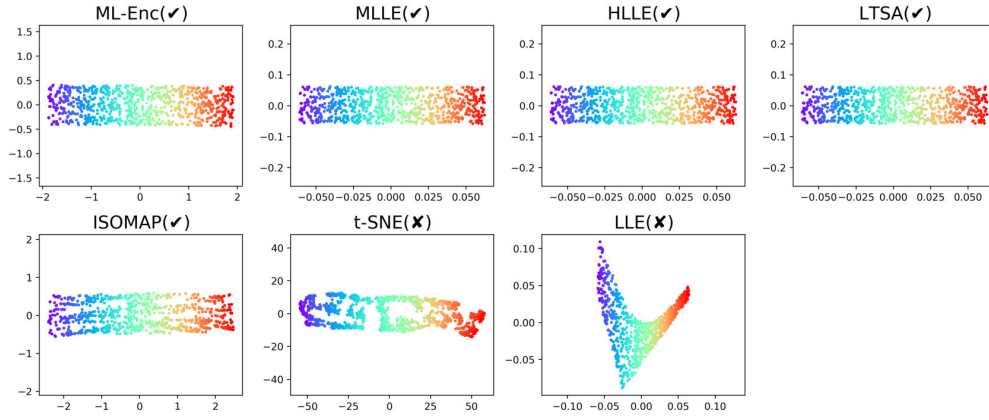
S-Curve (Seed=0)



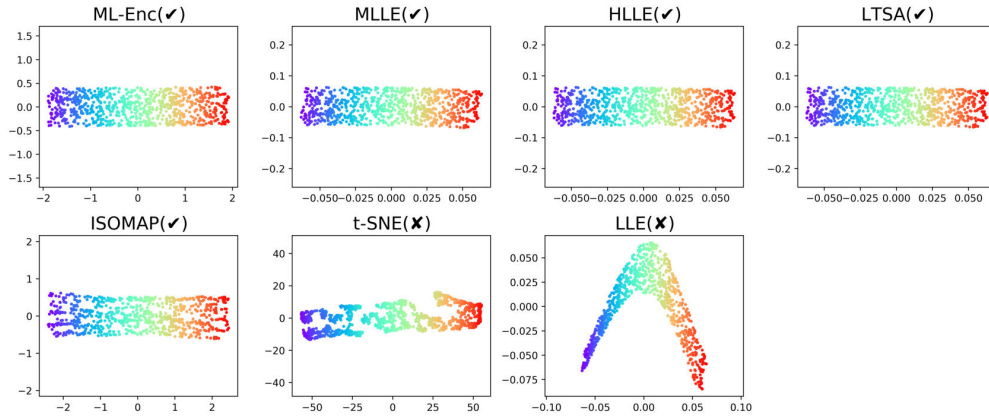
S-Curve (Seed=1)



S-Curve (Seed=2)

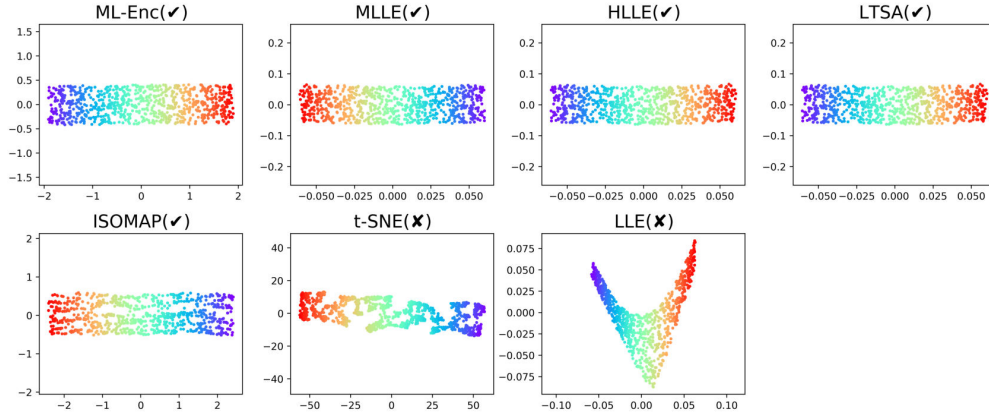


S-Curve (Seed=3)

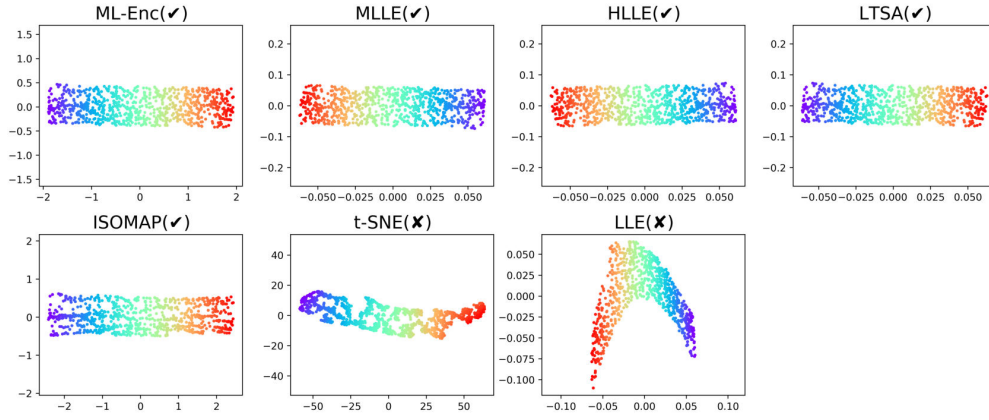




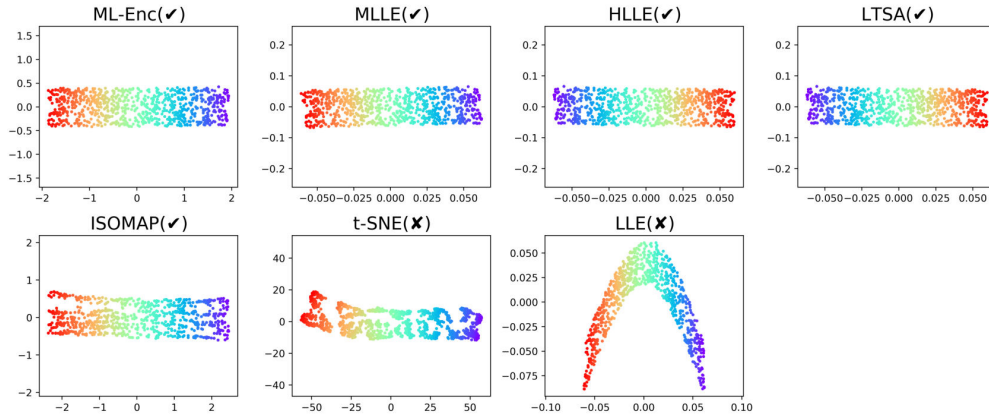
S-Curve (Seed=4)



S-Curve (Seed=5)

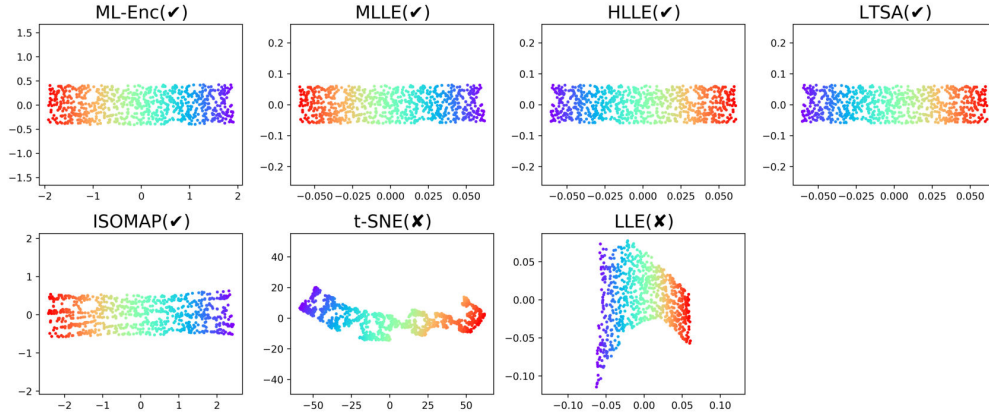


S-Curve (Seed=6)

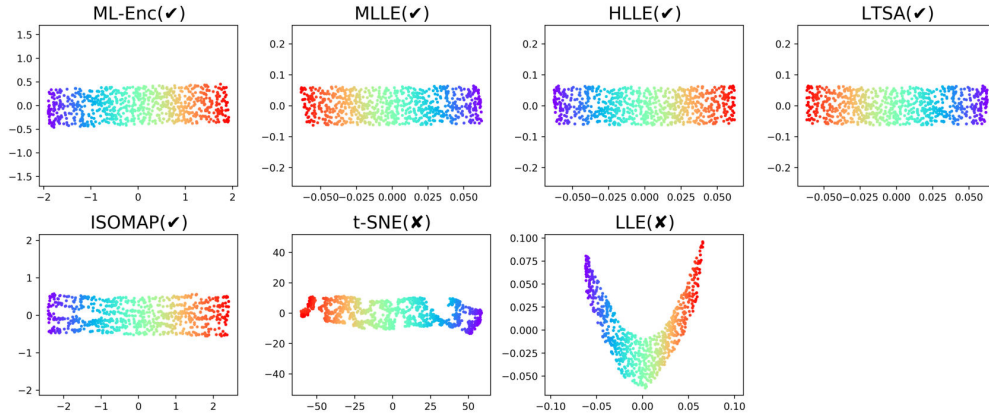




S-Curve (Seed=7)



S-Curve (Seed=8)



S-Curve (Seed=9)

